Eur. Phys. J. A **16**, 509–525 (2003)
DOI 10.1140/epja/i2002-10124-7

THE EUROPEAN PHYSICAL JOURNAL A

Enhanced neutron pair transfer and collective excitations in the system ^{206}Pb + ^{118}Sn at barrier energies

I. Peter[1], W. von Oertzen[2,3,a], S. Thummerer[2], H.G. Bohlen[2], B. Gebauer[2], J. Gerl[1], M. Kaspar[1], I. Kozhoukharov[1], T. Kröll[4], M. Rejmund[1], H.J. Wollersheim[1], and I.J. Thompson[5]

[1] Gesellschaft für Schwerionenforschung Darmstadt, Planckstraße 1, 64291 Darmstadt, Germany
[2] Hahn-Meitner-Institut Berlin, Glienicker Straße 100, 14109 Berlin, Germany
[3] Fachbereich Physik, Freie Universität Berlin, Germany
[4] INFN, Sezione di Padova,Via Marzolo 8, 35131 Padova, Italy
[5] Department of Physics, University of Surrey, Guildford GU2 7XH, UK

Received: 27 August 2002 / Revised version: 21 October 2002 /
Published online: 25 March 2003 –
Communicated by D. Schwalm

Abstract. At energies below the Coulomb barrier, neutron transfer and Coulomb excitation have been measured in a very heavy asymmetric nuclear system, in ^{206}Pb + ^{118}Sn. These are semi-magic nuclei showing super-fluid properties. Particle-γ coincidence techniques using 5 Euroball Cluster detectors (EB), combined in a set-up with the Heidelberg-Darmstadt NaI Crystal Ball (CB), have been used. Position-sensitive detectors allowed the observation of scattering processes covering angles from 110 up to 150 degrees. The fragments are identified via the known γ-decays of the lowest excited states using the high resolution of EB. Using the unique feature of the set-up with the CB, transfer to well-defined final channels with known quantum numbers is selected using the high-efficiency multiplicity filter of the CB with *no* second γ-ray, *i.e.* without feeding. The data are analysed using the semi-classical approach and transfer probabilities are obtained. Coulomb excitation has been analysed using known transition probabilities. The enhancement is deduced for the two-neutron transfer populating the low-lying super-fluid 2^+ states in ^{120}Sn and ^{116}Sn, while the 2n transition remains in the ground state for the ^{20N}Pb nuclei. Large enhancements up to $EF \simeq 10^3$ are observed. This is the first observation of neutron pair transfer enhancement for a heavy nuclear binary system with super-fluid properties with experimentally separated levels. The calculations with microscopic 2-neutron wave functions, with configuration mixing over six shell model configurations and using the coupled reaction channels approach, reproduce well the observed probabilities and the enhancement.

PACS. 24.10.Eq Coupled-channel and distorted-wave models – 25.70.Hi Transfer reactions

1 Introduction

Single and multiple transfer of neutrons between heavy super-fluid nuclei has been studied in recent decades to observe the "collective" enhancement in the pair transfer expected if nuclei with super-fluid properties are brought into contact [1–6]. Such cases are obtained for nuclei with open shells, *e.g.* isotopes in the Sn region (N = 50–82) and in the Pb region for $N < 126$. They show systematic properties of pairing "rotational" bands. The nuclei are represented in an approach with particle number violation, in analogy to the violation of spherical symmetry, and their masses (energies) can be seen to form a band as a function of pair number. Similar to the collective electro-magnetic transitions in spacially deformed nuclei, the collective transitions associated with the pairing field (namely the two-neutron transfer probability) are expected to be strongly enhanced [1–10]. Our task is to study neutron pair transfer between two super-fluid heavy nuclei below the Coulomb barrier in order to have cold reactions and to identify completely the final reaction channel. Due to the experimental difficulties with very heavy ions which make particle identification and the separation of final states populated in the binary reaction rather difficult, the definition of the experimental quantities and the enhancement connected with the two-neutron transfer have not been unique and a matter of varying arguments; the most recent compilation on this issue is given in refs. [4,5, 11,12]. In addition to these studies with spherical nuclei, neutron pair transfer into states of deformed nuclei along

[a] e-mail: oertzen@hmi.de

the rotational bands populated via Coulomb excitation has attracted a great deal of interest [13–16].

The determination of the *enhancement* (EF) of the two-neutron transfer is also the main subject of the present study. A rather simple *global* or *macroscopic* definition of the enhancement has been used in many experiments with no energy resolution but complete particle identification (for example, work based on radiochemistry, or using magnetic separation techniques), where the whole strength in the single- and two-particle transfer transitions has been measured [4,5]. In these cases the single-particle transfer strength appears to be governed by a sum rule for states at the Fermi surface. The two-particle transfer, viewed as a sequential process, is enhanced for the low-lying states, the 0^+ ground states (and the lowest 2^+ states), via interference terms acting constructively, due to the phases of the amplitudes in the single-particle states populated as intermediate steps in the first transfer process (see also the discussions in refs. [6,7,9,10]). This phenomenon of constructively acting phases in a mixed configuration is in fact the sign of a super-fluid configuration in a finite system [7]. For heavy-ion reactions the enhancement to be expected for the probability of the two-neutron transfer, as compared to the product (square) of the observed single-particle transfer probabilities, is then connected to the number of intermediate states [10]; experimentally, with this definition, small values of the macroscopic enhancement in the range of 2–5 are typically observed [4,5]. Larger enhancements would have to be attributed to additional effects, like dynamical configuration mixing and/or to contributions of a one-step two-nucleon transfer, whose conceptual description would be best given in terms of a macroscopic formulation of the pairing mode [5,6], which is related to the nuclear density at the surface.

Quite a few experiments concerning transfer reactions have been performed using *particle-γ coincidence techniques*, see references in the recent compilation [5] and refs. [12,13,16,17]. Position-sensitive Parallel-Plate Avalanche Counters (PPAC) are typically used to register the charged particles from binary reactions, such as Coulomb excitation and transfer processes. These also give access to the velocity vectors needed for the Doppler-shift correction of the measured γ-rays from binary processes, where fragments reach velocities of $v/c > 0.1$. With the high resolution of Ge detectors, unique identification of the reaction product is thus obtained by selecting a known γ-transition. A position-sensitive particle signal allows also the determination of the scattering angle, and this is used for the evaluation of transfer probabilities as a function of reaction angle and minimum distance. Recently, results for both spherical [17–19] and deformed nuclei [16] have been published.

For the study of pairing effects and the enhancement of pair transfer, heavy-ion–induced transfer offers considerable advantages, because it gives direct access to reaction probabilities using the semi-classical properties of the reaction, (discussed in sect. 2), just as in Coulomb excitation [5,8]. In these cases the scattering cross-section can be factorised from the reaction probability, and the results of the measurements can be given as transfer probabilities as a function of the minimum distances reached in the collision for various reaction angles and energies. Although the same distance parameters can be reached at higher energies for smaller angles, it is essential to have conditions for *cold reaction processes*, which is only possible for backward scattering where the *relative velocities* are small. In order to have cold reactions, the collision has to be chosen to have the kinetic energy as small as possible at the turning point, where the transfer takes place (see fig. 2 below). This is assured by choosing energies below the Coulomb barrier and scattering angles close to 180 degrees, at least larger than about 110 degrees.

In the work of Härtlein *et al.* [16] for reactions with very heavy projectiles and deformed nuclei, there was an additional feature which became possible with the use of the highly efficient Crystal Ball (CB) [20], namely the experimental selection of "cold" reactions. This is done by selecting, in addition to the high-resolution gamma-transition (in the Euroball (EB) detectors), events in coincidence with a specific multiplicity and sum energy gate from the CB. This allowed in their case, as an example, the selection of only rotational and *no vibrational excitations*. The latter have typically excitation energies larger than about 700 keV, as compared to the rotational energy transitions in strongly deformed nuclei (100–500 keV). The energy to break a pair is typically 2 MeV, which can be read from the differences in Q-values for transferring neutrons in odd and even numbers.

In the present experiment a corresponding approach with the multiplicity trigger of the CB detector is used for *transfer reactions between two spherical, but super-fluid nuclei*, to select among the cold reactions populating low-lying states, those transitions which correspond to the "supra-cold" transfer reactions leading to the lowest possible states. This experimental set-up opens the possibility for the first time to derive a *microscopic enhancement* for pair transfer in heavy-ion reactions. This is because with the high-resolution Ge γ-detectors (5 Euroball Cluster detectors, EB) in coincidence with particle detection devices and the 4π NaI Ball (the Heidelberg-Darmstadt Crystal Ball, CB), a uniquely defined transition can be picked out by *removing the feeding in both fragments* defined by the *CB multiplicity filter set to zero* (CB0). Thus, the high efficiency of the CB makes it possible to select a unique reaction channel defined by a transfer process to one low-lying state selected via the high-resolution EB-γ-spectrum. In the following the low-lying 2^+ states of the spherical nuclei ^{116}Sn and ^{120}Sn as well as of ^{204}Pb are used to select the 2n transfer reaction.

In fact it has been argued that these low-lying states of semi-magic nuclei form also a "super-fluid rotational band" as a function of pair number. The excitation energies of the first 2^+ states are almost degenerate in excitation energy for different isotopes, which has been noticed in earlier studies of the enhancement in (t,p) reactions [1–3]. An explanation is also given in terms of the excitation of d-bosons [21], or as an $l = 2$ wave on

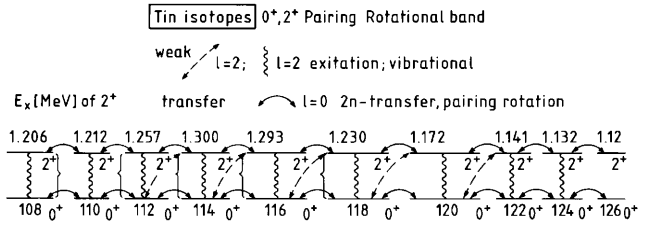

Fig. 1. Excitation energies of the low-lying 2^+ states in Sn isotopes, the energies are nearly constant, a fact which can be described as a pairing rotational band with an $l = 2$ wave of a super-fluid phase. Transfer routes are indicated.

the super-fluid phase [22]. To illustrate this point, we show in fig. 1 the energies of the low-lying 2^+ states in the chain of the Sn isotopes, with the possible transitions generated by inelastic excitation (Coulomb excitation) and the enhanced two-neutron transfer populating the 2^+ states. Similarly, the 2^+ states in the ^{20n}Pb isotopes (with $n < 206$) are almost degenerate in excitation energy. The explicit calculation of the wave functions of such 2^+ states in ^{206}Pb has been done by Igarashi *et al.* [23]; they show a degree of configuration mixing almost as large as for the 0^+ ground states.

Our measurements will give access to experimental quantities, from which we can derive a microscopic enhancement for the two-neutron transfer between two heavy nuclei, as originally done for the case of (t,p) reactions. The *microscopic definition of enhancement* has been introduced in the earlier work based on the (t,p) or (p,t) reactions, which is summarised in ref. [1]. In these reactions, the complete separation of final states is naturally achieved. There, comparison is made between *one* typical single-nucleon transfer transition and the two-neutron transfer between ground states ($0^+ \rightarrow 0^+$). However, due to the quantal properties of the light-ion reactions, recourse to DWBA calculations with optical model parameters for the initial and final channels is necessary. In order to extract enhancements, *the two-neutron transfer strength must be calculated in DWBA for one single-shell model configuration selected from the measured 1n transfer* and compared to the experimental value of the 2n transfer.

Although this procedure has sometimes been followed also for the case of heavy-ion reactions (see also our calculations in sect. 4.2), the semi-classical properties of these reactions and the use of transfer probabilities give direct access to the enhancement. The latter occurs in our case, because of the configuration mixing involved in the two vertices (two combinations of overlaps with super-fluid properties) contributing in the 2n transfer process. This microscopic definition for 2n transfer in heavy-ion reactions can now be tested with the work described here (a preliminary report has been given in ref. [18]), but without recourse to DWBA calculations.

The paper is organised in the following way. In sect. 2, we describe the dynamical conditions of the transfer process, which are needed to define the parameters in the semi-classical analysis of the experiment; these also helped to determine the proper choice of the incident energy and the angular range. In sect. 3, the experimental set-up is presented, the treatment of the raw data is discussed and the experimental results are shown in terms of transfer probabilities. The *enhancement* of the two-neutron transfer is deduced for the *cold* and for the *supra-cold* events. In sect. 4, the results for the transfer probabilities are compared with model calculations and with results of former works. Perspectives and conclusions are given in sect. 5.

Table 1. Q-values in MeV for the system ^{206}Pb + ^{118}Sn, shown as a function of the Sn-like transfer products.

A_1	116	117	**118**	119	120
Z_1					
$_{52}$Te	−12.65	−11.65	−6. 91	−7.03	−3.12
$_{51}$Sb	−8.89	−8.23	−5.02	−5.44	−2.73
$_{50}$**Sn**	**−2.42**	**−2.71**	**0.0**	**−1.48**	**1.01**
$_{49}$In	−4.82	−5.36	−3.37	−4.65	−3.33
$_{48}$Cd	−3.39	−4.77	−2.91	−5.41	−3.95

2 Semi-classical aspects of heavy-ion transfer reactions

2.1 Choice of the reaction and kinematic conditions

The system ^{206}Pb + ^{118}Sn has been chosen in order to observe an enhancement of the two-neutron transfer in optimum conditions. The Q-values of the system are shown in table 1, and since the values are of the order of 0 ± 3 MeV for neutron transfer reactions in both directions, these will be favoured. Proton transfer in any direction is blocked due to the large negative values. For the 2^+ states at typically $E_x \simeq 1.2$ MeV excitation, accordingly slightly more negative Q-values are relevant.

The chosen system is the heaviest asymmetric semi-magic system with closed proton shells and open neutron shells which can be studied. From previous works [1,23] it is known that the ground states and also the low-lying 2^+ states of such nuclei show strong configuration mixing. An enhancement in 2n transfer reactions between the low-lying states can be expected only in "cold" reactions, where the excitation energy of the two fragments will not be too high.

The incident energy has been chosen slightly below the Coulomb barrier, where the nuclear interaction between the nuclei is small and can be neglected in the dynamical description of the reaction. In addition, the reactions were observed at large scattering angles. Thus, the kinetic energy and the relative velocity between the nuclei at the turning points, where the transfer takes place, are as small as possible. For that reason, Sn nuclei were chosen as the projectile and Pb nuclei as the target, and the observation of the Sn nuclei is made at angles larger than 90°. The position-sensitive counters, the PPACs, were arranged in such a way that back-scattered Sn isotopes at angles from 80° to 150° could be observed. In this case the transfer will be as cold as possible and takes place between the lowest excited states.

Table 2. Energies for the system ^{206}Pb + ^{118}Sn, wave numbers k and Sommerfeld parameters η.

$E_{\rm lab}$ (MeV)	$E_{\rm c.m.}$ (MeV)	k (fm^{-1})	η
606	385	37.234	289
627	399	37.874	284

2.2 Classical orbits and matching conditions

We will discuss here reactions at energies where the nuclear interaction between nuclei can be regarded as a small perturbation or even be neglected. In this energy regime the heavy nuclei will move on trajectories determined by the Coulomb forces. The large masses also imply large charge products $Z_1 \cdot Z_2$ (with Z_1, Z_2 being the charges of the nuclei) and a very small wavelength λ. Thus the Sommerfeld parameter η becomes large. It is defined as

$$\eta = \frac{Z_1 Z_2 e^2}{\hbar v} = \frac{Z_1 Z_2 e^2 p}{2E\hbar} = \frac{R^0_{\rm min}}{2\lambda}\,. \qquad (1)$$

The following definitions are used: v is the velocity in the centre of mass (c.m.) system, E the energy in the c.m. system, p the momentum, and $\lambda = \hbar/k$ is the de Broglie wavelength. The corresponding values for the two energies chosen in our experiment are given in table 2.

The parameter $R^0_{\rm min}$ is the distance at closest approach in the scattering orbit for 180° scattering. The minimum distance is given by

$$R_{\rm min}(\theta, k, \eta) = \frac{\eta}{k}\left(1 + \frac{1}{\sin\theta/2}\right) = \frac{Z_1 Z_2 e^2}{2E}\left(1 + \frac{1}{\sin\theta/2}\right)\,. \qquad (2)$$

For reactions with $\eta \gg 1$, the processes can be described by semi-classical methods, because the form factors for reactions vary quite slowly as a function of $R_{\rm min}$ compared to λ. This will facilitate the discussion of the transfer process. In analogy to the approach used in Coulomb excitation, the calculation of the transfer cross-section $(\mathrm{d}\sigma/\mathrm{d}\Omega)_{\rm tr}$ can be factorised into a scattering cross-section $(\mathrm{d}\sigma/\mathrm{d}\Omega)_{\rm sc}$, a transfer probability $P_{\rm tr}(\theta)$, and quantal corrections for Q-value and angular momentum mismatch $F(Q, L)$:

$$(\mathrm{d}\sigma(\theta)/\mathrm{d}\Omega)_{\rm tr} = (\mathrm{d}\sigma(\theta)/\mathrm{d}\Omega)_{\rm sc} P_{\rm tr}(\theta) F(Q, L) \qquad (3)$$

This factorisation has been discussed in numerous publications [4,8,9,11]. The particular properties of the quantal correction factor $F(Q, L)$ and its refined details for reactions with separated final states in both fragments, as well as some discussion for reactions at higher energies are given in these references. The main effect actually comes from the Q-value mismatch, as shortly discussed below. In our case the experimental Q-values are very close to the optimum values. In the following, we define the reactions in the usual scheme as a + A = (b + c) + A → b + B = b + (A + c), where final states of the composite systems

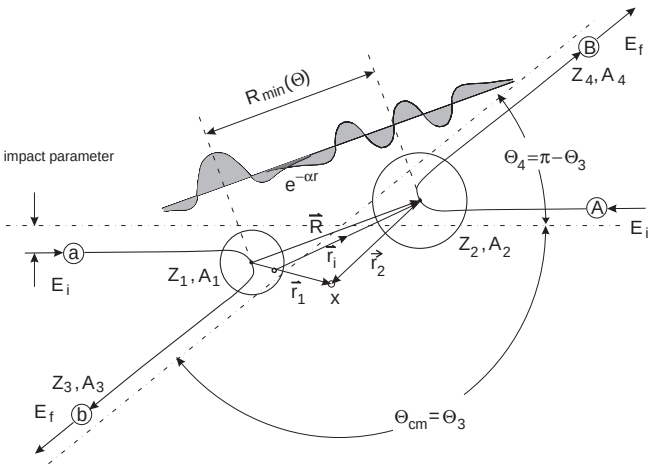

Fig. 2. Definition of quantities used in semi-classical conditions for transfer reactions. The figure depicts an orbit leading to large scattering angles for an energy below the barrier. The minimum distance, the scattering angle, the coordinates of the valence particle and the overlap of the tails of wave functions are illustrated.

(b + c) and (A + c), as well as of the core nuclei b and A, are populated after the transfer of c nucleons. In many experiments the states have not been separated. We also use (as in fig. 2) for the initial channel simply the definitions A_1 (= a) and A_2 (= A), and A_3 and A_4 for b and B, and for the nuclear charges Z_i ($i = 1, 4$), correspondingly.

As already stated, the Q-values for the transfer reactions are well matched in the chosen reactions, and no correction for mismatch using the function $F(Q, L)$ will be used in the final presentation of the experimental data (in sect. 3). The results will be given in terms of transfer probabilities $P_{\rm tr}(d_0)$ (as defined in eq. (3)), where the angle θ has been transformed to the distance parameter $d_0(R_{\rm min})$. In this approach the quantity $P_{\rm tr}(d_0)$ *becomes independent of the charge product and the incident energies*, thus the data will be shown always as a function of the minimum distance, with the parameter $d_0(R_{\rm min})$. We further have removed the dependence on the sizes of the nuclei by dividing out the well-known $A^{1/3}$-dependence. We define the overlap parameter d_0 by the following relation:

$$d_0(\theta) = R_{\rm min}(\theta) / \left(A_1^{1/3} + A_2^{1/3}\right)\,. \qquad (4)$$

In this way transfer probabilities in many systems have been compared in a systematic way covering a large body of experimental data [5,11]. In fact we have chosen *two* incident energies to test the independence of our results from variations of scattering angle or energy, when plotted as a function of d_0 in figs. 14, 15 below and others.

The macroscopically defined cold neutron transfer probabilities have properties which are related to universal behaviours of average nuclear quantities, like radii and the density of valence particles at the nuclear surface. These reflect the overall evolution of nuclear radii, described by the $A^{1/3}$ factor, which disappears for the transfer probabilities once this factor is divided out and the result is given for definite values of the overlap parameter.

In eq. (3) the definition of the scattering cross-section $(\mathrm{d}\sigma/\mathrm{d}\Omega)_{\mathrm{sc}}$ is extended to energies slightly above the barrier, where absorption takes place via a larger number of reaction channels. This results in an absorptive potential (see, in particular, discussions in refs. [8,11] and [9]). In the semi-classical approach a quantity called absorption probability $P_{\mathrm{abs}}(\theta)$ is defined. The scattering cross-section is obtained in terms of the Rutherford cross-section and a function P_{abs} describing the absorption:

$$\left(\frac{\mathrm{d}\sigma(\theta)}{\mathrm{d}\Omega}\right)_{\mathrm{sc}} = \left(\frac{\mathrm{d}\sigma(\theta)}{\mathrm{d}\Omega}\right)_{\mathrm{R}} [1 - P_{\mathrm{abs}}(\theta)] \,. \qquad (5)$$

This absorption factor acts in all reaction processes and cancels out once the ratios for the probabilities are calculated.

An important aspect of quasi-elastic nucleon transfer is the change of the properties of the two-body systems and, in particular, of their dynamic parameters due to the transfer of mass, charge, angular momentum and energy. This leads to matching conditions for the external scattering states (wave functions) and as well to conditions for the intrinsic bound states between which nucleons have to be exchanged. Deviations from the optimal matching conditions result in a reduced cross-section, which can be cast into the quantal correction factor $F(Q, L)$, introduced in eq. (3). For charged-particle transfer, often an optimum Q-value, Q_{opt}, is defined, which is discussed in more detail in refs. [8,9,11].

The matching aspect is completely analogous to the matching problem discussed in Coulomb excitation [8], namely a quantal correction is needed if the scattering orbits do not match due to changes in the variables, which define the scattering orbit. Evidently, for neutron transfer $Q_{\mathrm{opt}} \equiv 0$ is obtained. The present system has been chosen in such a way that the Q-values encountered in the various neutron transfers (neutron stripping and pick-up referring to the projectile ^{116}Sn) are around zero or slightly more negative (-2.0 MeV), the values are given in table 1. With these small deviations of the Q-values from the optimum values the corrections become smaller than a factor two, and in the discussion of the enhancement no corrections for the factor $F(Q, L)$ are introduced.

2.3 Multi-nucleon transfer and enhancements

In the semi-classical approach, sequential transfer (with, for example, equal probabilities in the individual steps) will produce multi-nucleon transfer; its final probability can be obtained by multiplication of probabilities $P_{x\mathrm{n}} = (P_{1\mathrm{n}})^x$, or written as $\prod_{i=1}^{x} P_{i\mathrm{n}}$, for a prediction of the probability of an independent sequential transfer of x nucleons. However, correlations between nucleons leading to configuration mixing, can induce a strong enhancement in sequential pair transfer and can also introduce an additional (enhanced) contribution of one-step pair transfer. The transfer of several pairs between two heavy nuclei in the enhanced situation produces a unique effect, corresponding to a larger flow of nucleons, which will be

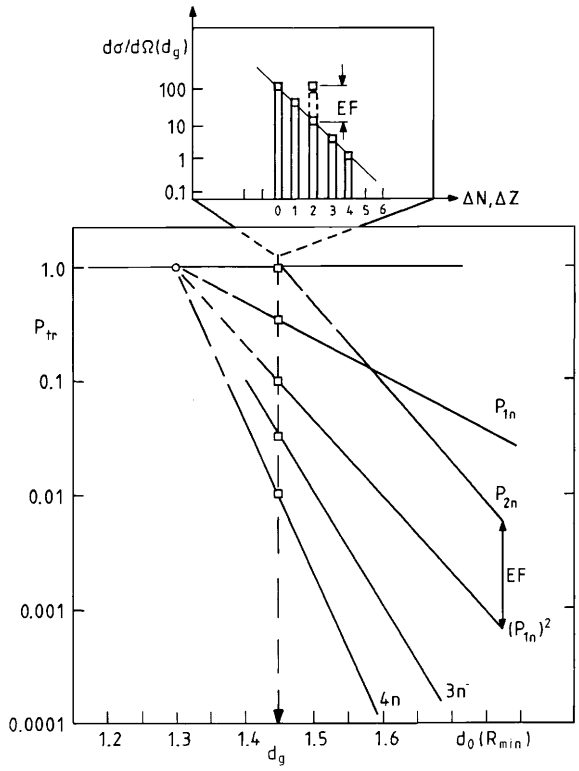

Fig. 3. Schematic representation of transfer probabilities for the idealised cases of sequential multi-neutron transfer, if for each single nucleon step the same absolute value and the same dependence on the distance between the nuclei (on the overlap parameter d_0) are observed. The case of an enhanced probability for two-neutron transfer is shown, the factor of the parallel shift defines the enhancement factor EF.

stronger than that produced by the transfer of independent nucleons by orders of magnitude [4,5,24]. This is called a "super-current" just as in the case of a super-current carried by "Cooper pairs" (electrons). Based on previous experience [1,4,9], the *enhancement factor EF* for two-nucleon transfer due to pairing can be defined simply in the semi-classical approach, as

$$P_{2\mathrm{n}} = EF \cdot P_{1\mathrm{n}}^2 \,. \qquad (6)$$

This expression implies that with $EF > 1$ more nucleons are transferred as pairs as compared to the case of *independent* multiple single-particle transfer.

In the ideal case, the dependence of the transfer probability as a function of distance has a decay slope α given by the following definitions (see also figs. 2 and 3):

$$P_{\mathrm{tr}}(d_0) \simeq \exp(-2\alpha d_0), \qquad \alpha = (2\mu E_{\mathrm{B}})^{1/2}/\hbar \,. \qquad (7)$$

Here μ stands for the reduced mass of the transferred particle and E_{B} for its binding energy. For overlap distances with $d_0 > 1.3$ fm, the decay constant α can be predicted from simple considerations of the tails of the bound-state wave functions [11,12]. For the two-neutron transfer, $\alpha_{2\mathrm{n}}$ is related to the one-neutron transfer by the simple relation $\alpha_{2\mathrm{n}} = 2\alpha_{1\mathrm{n}}$. We can draw in fig. 3 a fan

of exponential curves representing the transfer probability for different steps in multi-neutron transfer with the enhanced probabilities shifted parallel in a logarithmic scale (see also figs. 12, 13, 14 and 15 below for the experimental results of one- and two-neutron transfer).

The definition of the *enhancement factor EF* can be made for selected (separated) two-nucleon (for example, the 0^+ to 0^+) transitions [1,5], relative to *one single-nucleon* transition; this we have called the *microscopic* definition in the introduction. The usually adopted *macroscopic* definition of EF in heavy-ion reactions is obtained if the transfer strength is taken as the sum over the states populated in single-nucleon transfer and compared to the sum of states populated in pair transfer. The latter will be predominantly the 0^+ and the 2^+ states, with some contributions from other low-lying states. In our case, the gamma-decay feeding from higher-lying states into the selected lowest 2^+ state, is observed, but later removed via the CB anticoincidence.

For a purely sequential process, the enhancement of $0^+ \rightarrow 0^+$ transitions in two-nucleon transfer is produced by the coherent action of the amplitudes of states populated in the first step of the single-neutron transfer, namely those single-particle states contributing to the configuration mixing responsible for the super-fluid phase. The EF factor is then determined by the number of coherent intermediate states populated in single-nucleon transfer (a discussion of this aspect is given in ref. [10]) and an example of such a calculation can be found in ref. [7]. In cases of large configuration mixing over two major shells with opposite parity, the one-step contribution, namely the transfer of a neutron pair, can dominate by one order of magnitude (see, for example, ref. [25]). In sect. 4.2, explicit calculations for the present case will be shown.

3 Experimental set-up and results

3.1 Experiment

The experiment has been performed at the UNILAC at GSI-Darmstadt with a beam of ^{118}Sn at two energies below the Coulomb barrier, at 5.14 MeV/u and 5.32 MeV/u, and with a target of ^{206}Pb consisting of a 400 μg/cm^2 Pb layer and a carbon backing. The two energies have been chosen in order to have an independent variation of the dynamic parameters. The experimental set-up is shown in fig. 4. It consisted of 5 Euroball Cluster detectors (EB), and the Crystal Ball (CB) [20] for measuring γ-rays. For charged-particle detection, in addition three Parallel-Plate Avalanche Counters (PPACs) for measuring the recoil nuclei were built [26].

The EB Clusters, consisting of 7 Ge detectors each, were arranged in a ring at about 150° to the beam direction and surrounded by a BGO shield for the suppression of Compton scattering out of the clusters, which would lead to incomplete detection of γ-rays. The most important feature of the EB ring was the high-energy resolution of 2.5 keV and the total photopeak efficiency of 2.2% for

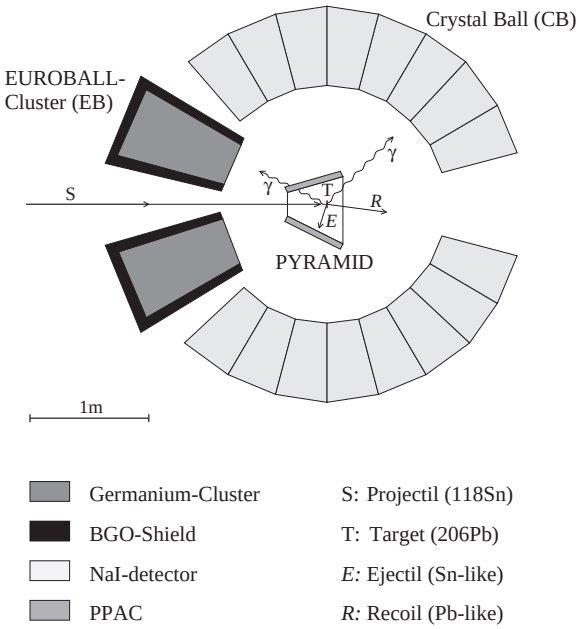

Fig. 4. Schematic view on the experimental set-up with Euroball detectors, the parallel-plate detectors (Pyramid) and the Crystal Ball.

a γ-energy of 1.33 MeV. The CB, with an energy resolution of 90 keV (for a γ-energy of 1.33 MeV) consisting of 130 NaI detectors was covering a large fraction of the remaining solid angle. The combination of the two systems gives a high total interaction efficiency of 80% for γ-rays).

The PPACs were integrated in a pyramidally shaped scattering chamber PYRAMID [26,27] and were used to measure the position of the scattered Sn-like isotopes over a wide angular range from 80° to 150° with a position resolution of 1 mm. The particle-γ coincidence technique, the coincident measurement of a scattered Sn isotope and at least one γ-ray in the EB was used to collect data. Due to the high resolution of the EB, the different transfer channels or inelastic scattering (Coulomb excitation) can be identified with their known γ-decays of the lowest excited states in one nucleus (Sn or Pb). The high accuracy of the position measurement of the scattered Sn-like isotopes with the PPAC allows to determine the scattering angle and thus to perform the needed Doppler correction of the measured γ-rays as well as to determine the reaction angle (and the overlap parameter d_0). With the high total interaction efficiency of the Crystal Ball, it is possible to set conditions on the γ-sum energy and/or the γ-multiplicity of a reaction [16] and thus to select different reaction mechanisms, *i.e.* to select the "supra-cold" transfer, as will be discussed in sect. 3.3.

3.2 Treatment of EB-γ-ray spectra

The detection of γ-rays, in particular with Ge detectors, is always accompanied by unavoidable Compton scattering of the γ-rays out of the detector material. As a

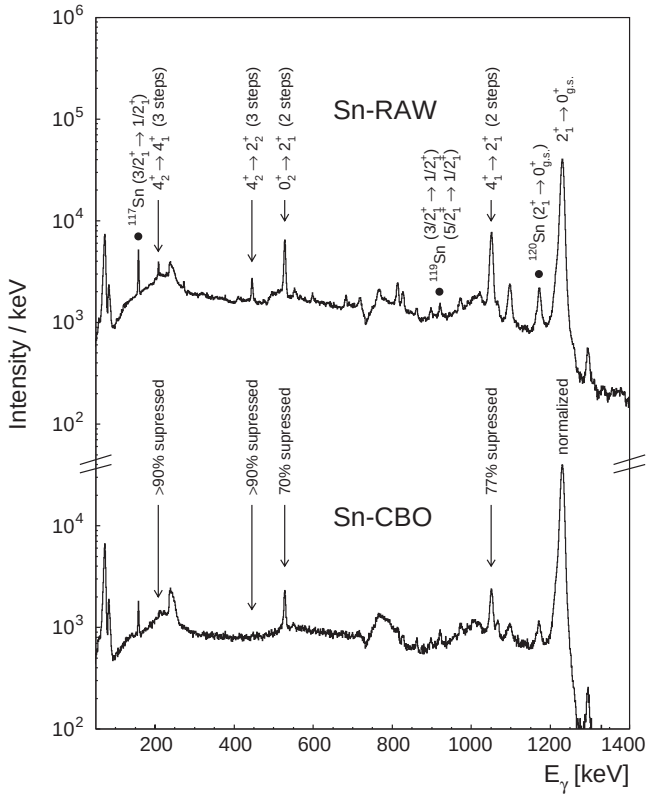

Fig. 5. γ-ray spectra from EB Clusters, Doppler-corrected for Sn nuclei. The upper spectrum is obtained without any conditions set on the CB (Sn-raw), the lower spectrum with the CB in anticoincidence (Sn-CB0) normalised to the $2_1^+ \rightarrow 0_{\rm g.s.}^+$ transition in ^{118}Sn at an energy of 1230 keV. Strong lines from multiple Coulomb-excitation reactions of ^{118}Sn are marked and their suppression due to the CB filter can be seen. The strongest transitions of different transfer products are indicated by black dots.

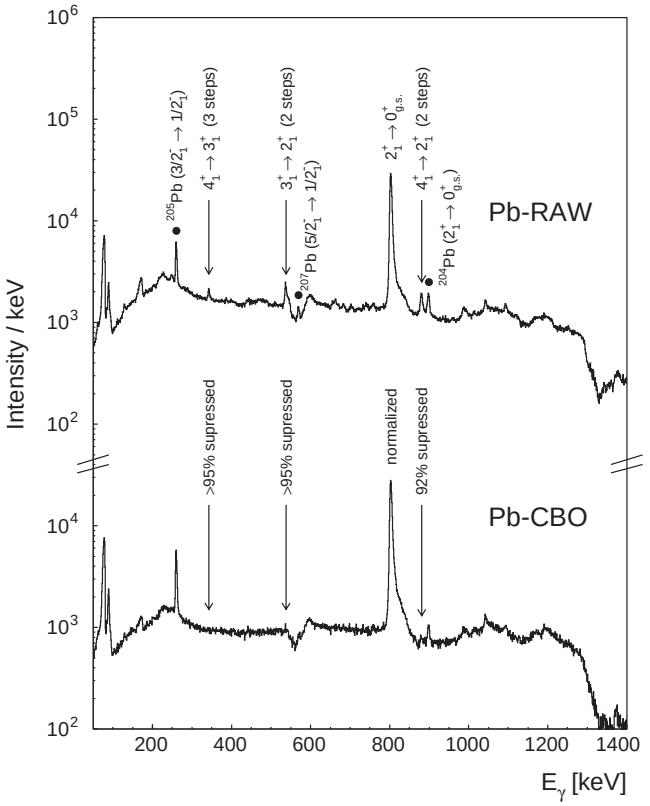

Fig. 6. Same spectrum as in fig. 5, Doppler-corrected for Pb isotopes.

consequence, the photopeak efficiency decreases and the background in the γ-spectra increases. With the EB Cluster a large fraction of those Compton events could be recovered. In the so-called Add-Back algorithm, the γ-energies of nearest-neighbour Ge detectors within one EB Cluster are added up and treated as *one* γ-ray afterwards, *e.g.* for the Doppler-shift correction (see below). Performing the Add-Back algorithm in that way, the photopeak efficiency of the experimental data could be improved by 40% for the energy of 1230 keV [26].

In the present experiment, the γ-rays were emitted by the fragments in flight and thus the measured γ-energies were strongly Doppler-shifted. The consequence is a bad γ-energy resolution in the raw EB-spectra, which makes the identification of different reaction channels impossible. Measuring the position of the scattered Sn isotope in the PPACs and the direction of the emitted γ-ray (determined by the position of the detecting EB-γ-detector), the vectors of the emitting particles and of the γ-ray could be reconstructed. By knowing these vectors and assuming a binary reaction (including quasi-elastic scattering), a correction of the Doppler shift has been performed and a resolution better than 1% at a γ-energy of 1230 keV has been obtained, which was sufficient for the identification of reaction channels.

One problem still remains: it is in principle not possible to decide if a γ-ray was emitted by a Sn isotope or a Pb isotope. For that reason, the Doppler-shift correction was performed two times, once assuming the γ-ray was emitted by a Sn isotope and, second, assuming that it was emitted by a recoiling Pb isotope. In this way, always two spectra are obtained, one showing sharp transitions of Sn isotopes and the other showing sharp transitions of Pb isotopes. In the upper parts of figs. 5 and 6 the EB-spectrum is shown for a Sn correction and a Pb correction, respectively.

To reduce the background of the Sn-spectrum those γ-energies which were identified as the most prominent, the inelastic Pb transitions (*e.g.*, $2_1^+ \rightarrow 0_{\rm g.s.}^+$ at 803 keV in ^{206}Pb) were not further included after performing the Pb-Doppler correction. This explains the artificial dip at an energy about 700 keV in the Sn-spectrum. The background in the Pb-spectrum was reduced in the same way. In accumulating off-line the spectra, the events at energies of γ-rays were not incremented if they belonged to the three strongest transitions in the Sn-spectrum ($2_1^+ \rightarrow 0_{\rm g.s.}^+$ at 1230 keV, $4_1^+ \rightarrow 2_1^+$ at 1050 keV and $0_2^+ \rightarrow 2_1^+$ at 528 keV, all in ^{118}Sn). The corresponding dips in the Pb-spectrum are seen at energies around 550 keV, 1100 keV and 1300 keV.

3.3 CB filter for the selection of "supra-cold reactions"

Reactions at low incident energies, as in the present case, are defined as "cold reactions" if only states with low excitation energies in the nuclei are populated. Due to the choice of the incident energies and the observation of large scattering angles, in the present experiment indeed mainly cold reactions were observed. This is reflected in the EB-spectra showing only a few-phonon excitation states (figs. 5 and 6) and only some γ-rays for a few transfer reactions.

The high interaction efficiency of the CB allows the accurate measurement of the sum energy and multiplicity of the associated γ-rays. The CB can thus also be used as a highly efficient anticoincident filter. Demanding *no measured γ-ray* in the whole CB, it is possible to select "supra-cold reactions" out of the cold reactions in the EB-spectra. The EB-spectra with the CB in anticoincidence (defined as CB0) are shown in fig. 5 in the lower part for Sn and in fig. 6 for Pb. Compared to the non-filtered spectra (on top of each figure) lines which correspond to two- and higher-phonon excitations in Coulomb excitation are suppressed with respect to the $2_1^+ \rightarrow 0_{\text{g.s.}}^+$ transition. For Sn the two lowest-lying two-phonon states are suppressed by 70% and 77%, the observed three-phonon states by more than 90%, respectively. The suppression factor will depend on the γ-multiplicity in the reaction channel. For Pb every more-phonon excitation is suppressed by more than 90%. Taking into account these values and the multiplicity distribution for the transfer channels, one can conclude that any feeding into the lowest-lying states of the transfer channels is suppressed by more than 85%. Thus in the case of *supra-cold reactions* (CB0), the transfer cross-sections correspond predominantly to transitions populating *the selected state* combined with the *ground-state to ground-state transition* in the recoiling partner nucleus.

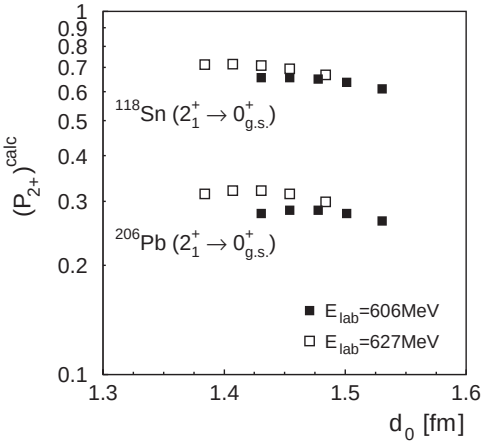

Fig. 7. Excitation probabilities of the $2_1^+ \rightarrow 0_{\text{g.s.}}^+$ transitions in ^{118}Sn and ^{206}Pb as a function of d_0.

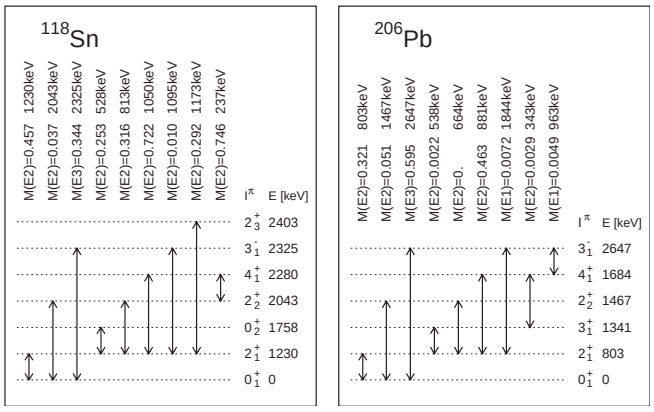

Fig. 8. Excitation energy of states in ^{118}Sn and ^{206}Pb and their couplings, and with values of the matrix elements from ref. [28] used in the Coulex calculations, discussed in sect. 4.1.

3.4 Determination of absolute cross-sections and reaction-probabilities

To overcome efficiency variations in the PPACs, *e.g.* due to target shadowing, the γ-yields of the transfer lines were normalised to the Coulomb excitation transition of the lowest 2^+ state (1230 keV), to the 0^+ ground state in ^{118}Sn, and the lowest 2^+ state in ^{206}Pb (803 keV), respectively (see fig. 7). The cross-sections for these transitions can be obtained with high accuracy from Coulomb excitation calculations. For the determination of absolute cross-sections and transfer probabilities the measured excitation probabilities (yields) as a function of scattering angle of these first 2^+ states in ^{118}Sn and ^{206}Pb are compared with calculations based on multiple Coulomb excitation which contain up to three phonons and several parallel feeding routes (see fig. 8). Because the $B(E2)$-values entering the calculation are known from previous work [28], we can *define with the Coulex cross-sections the absolute scale*, and obtain access to the absolute elastic and transfer cross-sections. In the extraction of the transfer probabilities (eq. (3)) we have to remember that the absorption is present in both the Coulex yields and the transfer yields. It is therefore cancelled in the experimental ratios of transfer/Coulex which are used as primary data. This procedure of determining transfer probabilities as a function of d_0, with values of d_0 reaching well into the region of absorption, has been shown to give good results in many cases [5,12,9], provided that sufficiently small energies are used and the absorption is not larger than about 95%.

For the presentation of the data in terms of transfer probabilities, $P_{\text{tr}}(d_0)$, as a function of nuclear distances, the differential range Δd_0 per data point was chosen to be $\Delta d_0 \simeq 0.025$ fm. These uncertainties are shown later as horizontal error bars at the experimental points like in figs. 9, 10 and 12 up to fig. 18 in later sections. The angular resolution of the particle detection device introduces an error which is considerably smaller. The minimum distances covered in the present experiment are in the range of $d_0 = 1.38$ fm–1.53 fm. Absorption into neutron transfer channels starts typically at $d_0 \simeq 1.5$ fm, and more complicated nuclear processes set in at values of d_0 around 1.4 fm [4,5].

3.5 Results for inelastic scattering

From the EB-spectra shown in the upper parts of figs. 5 and 6, the γ-yields of states in ^{118}Sn and ^{206}Pb populated by inelastic scattering were determined as a function of d_0. These yields are normalised to the $2_1^+ \rightarrow 0_{\mathrm{g.s.}}^+$ transitions in both Sn and Pb and the ratios could be reproduced very well by multiple Coulomb excitation calculations (see fig. 9), which are described in sect. 4.1, the transitions included are shown in fig. 8, together with the $M(E2)$ and $M(E3)$ values from ref. [28].

The results shown in fig. 9 show that, for Pb, the deviation between the experimental data and the calculation was less than 5%; for Sn, in some cases a deviation up to 50% was observed. This, however, has almost no influence (less than 1%) on the calculated probability $P_{2^+} = \sigma_{2^+}/\sigma_{\mathrm{el.}}$ of the $2_1^+ \rightarrow 0_{\mathrm{g.s.}}^+$ transition, which is shown in fig. 7, because the total feeding into the 2_1^+ state remains nearly constant. This was ascertained by changing the values of the matrix elements in the calculation (see sect. 4.1). Relying on the accuracy of this calculation, finally excitation probabilities can be extracted by multiplying the experimental data with the calculated $2_1^+ \rightarrow 0_{\mathrm{g.s.}}^+$ probability. They are presented in fig. 10 for both Sn and Pb nuclei.

3.6 Results on transfer reactions

One- and two-neutron transfer as cold reactions have been identified in both directions via the characteristic γ-transitions in the EB-spectra. In figs. 5 and 6 the strongest (and lowest) transitions are marked in the Sn branch and in the Pb branch, respectively. We show in fig. 11 the relevant level schemes of the transfer products with the γ-transitions marked, for which the selection in the EB γ-decay spectra has been made. Transfer probabilities as a function of d_0 have been derived from the γ-yields together with Coulomb excitation calculations as described in sect. 3.4. Among the γ-transitions there are only a few strong candidates in the 1n transfer channel which can be used to determine the 1n transfer probabilities. The situation is much simpler for the 2n transfer. There we are able to select unique 2^+ transitions, in ^{114}Sn, ^{120}Sn, and ^{204}Pb, respectively. The corresponding γ-transitions are shown in fig. 11. In figs. 12 and 13 we first show the overall result for cold transfer without any condition on the CB. These probabilities can be considered to represent the macroscopic values for cold transfer, which are typically obtained in experiments with magnetic spectrometers [5,9,24]. They contain partially the γ-decay feeding from higher-lying states; however, some transfer branches are missing, such as those leading directly to the ground states. The present overall transfer probabilities are thus typically a factor 3–5 smaller than those from the systematics cited in ref. [5].

In selecting the CB filter condition (CB0), the direct population of the state whose γ-decay is chosen in EB is obtained. Depending on whether the γ-feeding is strong or the direct population is strong, the difference between the

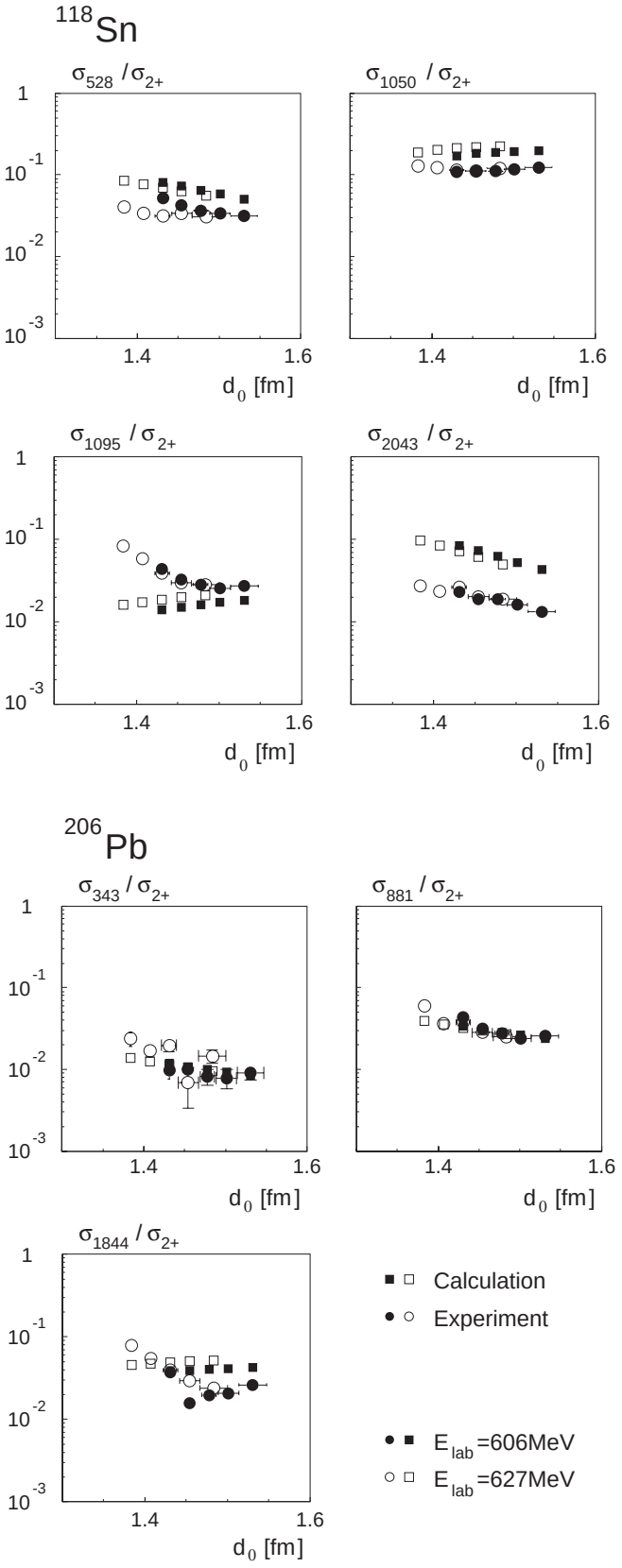

Fig. 9. Measured and calculated γ-yields (σ_{keV}) of states in Sn and Pb normalised to the corresponding $2_1^+ \rightarrow 0_{\mathrm{g.s.}}^+$ transition (σ_{2^+}) from inelastic excitations as a function of the overlap distance d_0.

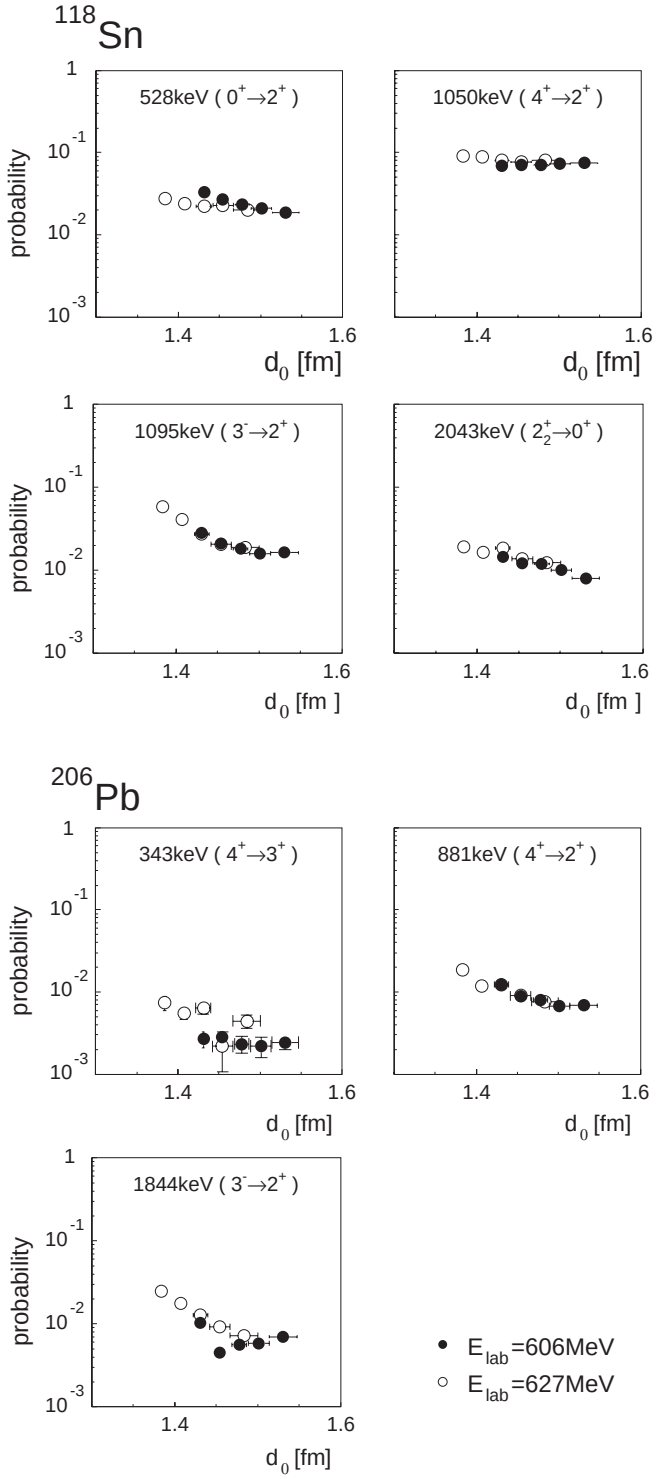

Fig. 10. Excitation probabilities of γ-transitions after inelastic excitation in the collision in the system ^{206}Pb + ^{118}Sn obtained from the experimental γ-spectra.

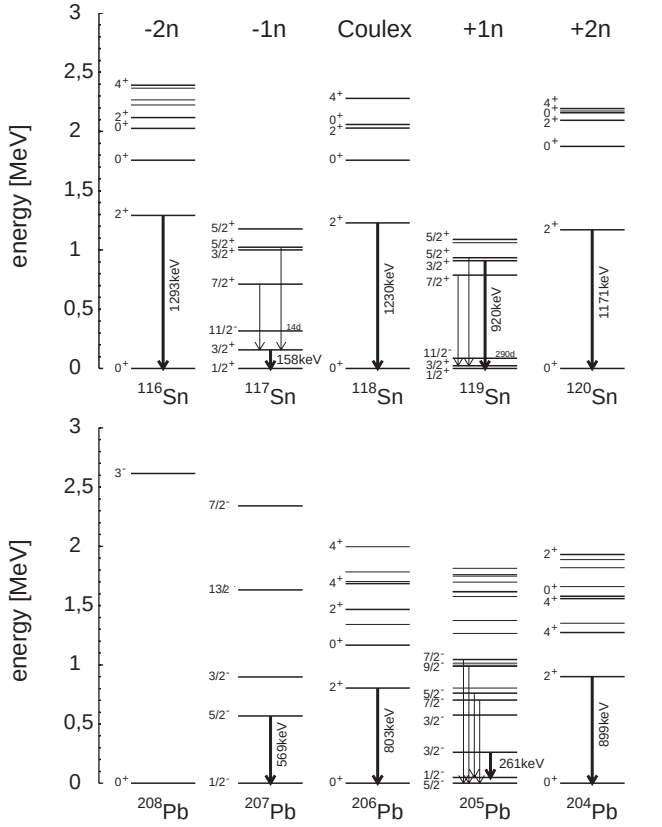

Fig. 11. Level schemes and γ-transitions which are used in the selection from the EB-spectra for fragments formed in 1n and 2n transfer reactions leading to the isotopes $^{116\text{-}120}$Sn and $^{204\text{-}208}$Pb. Only the strongest transitions are indicated, including the inelastic channels.

"raw" γ-ray yield and that with the CB filter may vary. We are interested in the selection of a typical single-particle state; the fact that the γ-transition is easily observed, already implies that we will choose a strong transition. Later in tables 3 and 4, the spectroscopic factors and the calculated cross-sections of the most important states will be given.

The result for the supra-cold reactions, *i.e.* with the CB in anticoincidence (CB0) (see sect. 3.3), are shown for 1n and 2n transfers in figs. 14, 15 and 18 (below). The predicted slopes from eq. (7) are indicated and are in good agreement with the experimental data, and they are independent of the incident energy and also identical to those of the data without the CB filter. This gives strong support to the claim that in the experiment proper conditions for cold reactions have been chosen. With the differences of the results with or without the CB in anticoincidence, we can judge to what extent the transfer took place directly into the selected state, and how much feeding from higher states has occurred.

From the data the enhancement factors EF can be derived by determining the parallel shift of the 2n transfer probability compared to the square of the 1n transfer probability (see fig. 18 in sect. 4.4). The anticoincidence with the CB also defines the quantum state of the partner nucleus, which must be the ground state for the no feeding case. This is not strictly true for ^{119}Sn and ^{205}Pb, because both nuclei have a first-excited state at a very low excitation energy and rather high spin, and thus with very long lifetimes, these cannot be removed with the CB. Those states are not excluded with the CB filter and the populated state of this nucleus as a "partner nucleus"

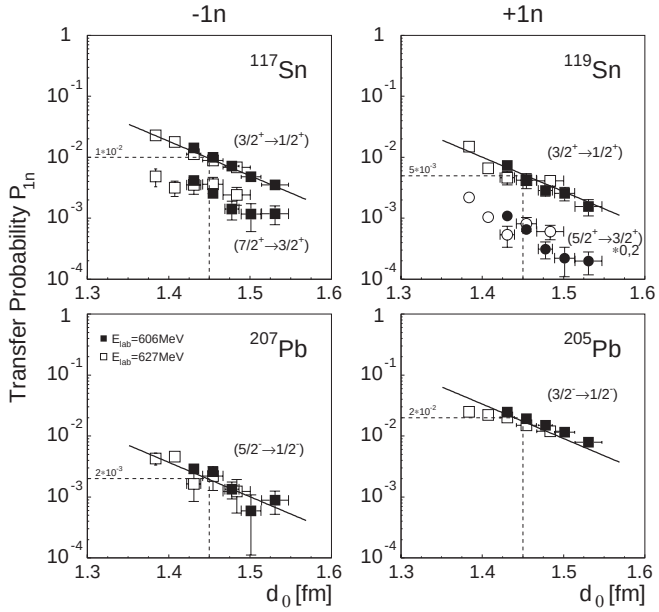

Fig. 12. Summary of measured one-neutron transfer-probabilities (P_{1n}) as a function of the inter-nuclear distance determined by the parameter d_0. The left column shows the neutron transfer from Sn to Pb, the right column vice versa. Filled symbols refer to a bombarding energy of 5.14 MeV/u, open symbols to 5.32 MeV/u. The nuclei are identified by their characteristic γ-transitions indicated in fig. 11, from the spectra shown in figs. 5, 6. The continuous lines show the theoretically predicted slopes of the 1n transfer probability. The dashed lines indicate the measured probabilities for a distance parameter $d_0 = 1.45$ fm.

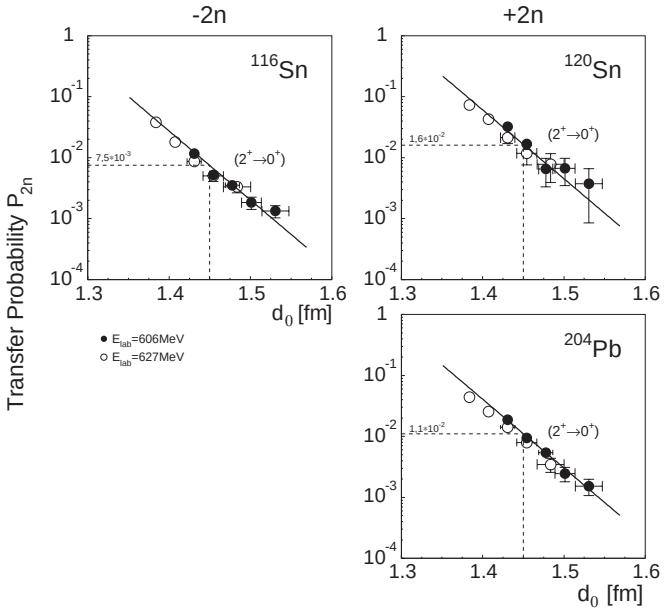

Fig. 13. Summary of measured two-neutron transfer probabilities (P_{2n}) for cold transfer as a function of the overlap parameter d_0. For further explanations see fig. 12.

becomes less well defined, *i.e.* a sum over two or three states, and the population of the single-particle strength summed with these excited states must be assumed. However, the contribution of these long-lived isomers appears to be rather small, because of their high spins.

For our purpose to determine the enhancement, we find an ideal and clean case for the 1n transfer with the γ-transition $3/2^+ \rightarrow 1/2^+$ in ^{117}Sn with the partner ^{207}Pb, and for the 2n transfer with the $2^+ \rightarrow 0^+$ gamma-decay in ^{116}Sn with the partner ^{208}Pb. In this case, the CB0 filter can determine exactly the quantum numbers of both partner nuclei and for this case we obtain from the data of the supra-cold reaction the microscopically defined enhancement factor as $EF = 900$. This is shown in fig. 18 below.

4 Analysis and discussion

4.1 Multiple Coulomb excitation

The calculation of the γ-decay intensities needs a coupled-channels calculation for multiple Coulomb excitation and the subsequent decay processes. The relevant programs are described in ref. [29]. For the multiple Coulomb excitation many matrix elements between the important low-lying states are needed. As already stated, the routes and the reduced matrix elements $B(El)$ for ^{118}Sn and ^{206}Pb are taken from ref. [28], and they are given in fig. 8.

A test of the validity of these calculations is obtained with the comparison of the measured and calculated γ-yields normalised to the $2^+ \rightarrow 0^+$ transitions (see sects. 3.4, 3.5 and fig. 9). Furthermore, the ratio of the 2^+ excitations in ^{118}Sn and ^{208}Pb between experiment and calculation was compared. With a deviation of less than 3%, they were in very good agreement.

4.2 DWBA and CRC calculations for two-neutron transfer

We have used the coupled-reaction code FRESCO [30] to calculate absolute cross-sections for 1n and 2n transfers by using known spectroscopic factors as compiled in the Nuclear Data sheets [31]. The calculation proceeds in the usual way for heavy-ion reactions [5], namely that for the 1n transfer the product of the spectroscopic amplitudes of the neutron in the two states in the two fragments has to be given for the chosen transition. In tables 3 and 4 the relevant information has been compiled, where the spectroscopic amplitudes of the states and the calculated cross-sections are given. We show the coupling scheme with the final choice of the single-particle transitions to select the binary channel in figs. 16 and 17. The peaks in the "raw" spectrum and the corresponding cross-sections are related to combinations of the (excited) states in the two odd-mass nuclei of the binary reaction, which spans a matrix of cross-sections (for example 6×6, for six configurations). Such a matrix has actually been calculated in the previous work for the study of neutron transfer in the ^{112}Sn + ^{120}Sn reaction [9].

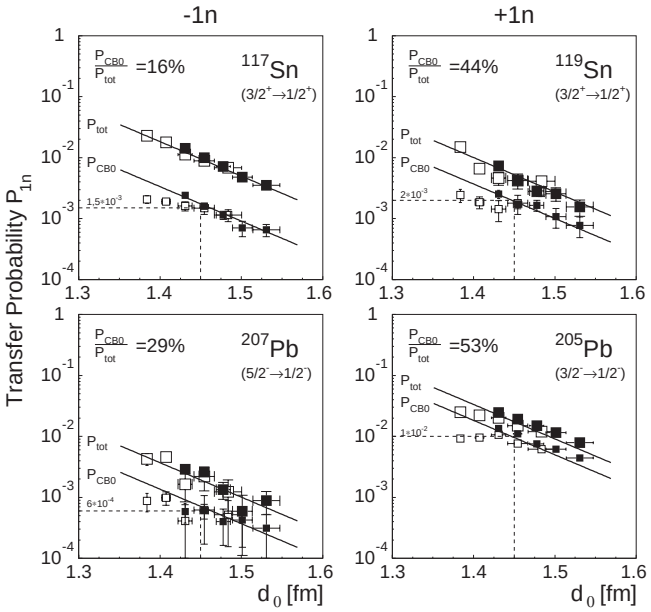

Fig. 14. Measured one-neutron transfer probabilities for the channels selected via the indicated γ-transitions as a function of the overlap parameter d_0 without any condition ($P_{\rm tot}$) and with the Crystal Ball in anticoincidence ($P_{\rm CB0}$). The percentage of the supra-cold component is indicated.

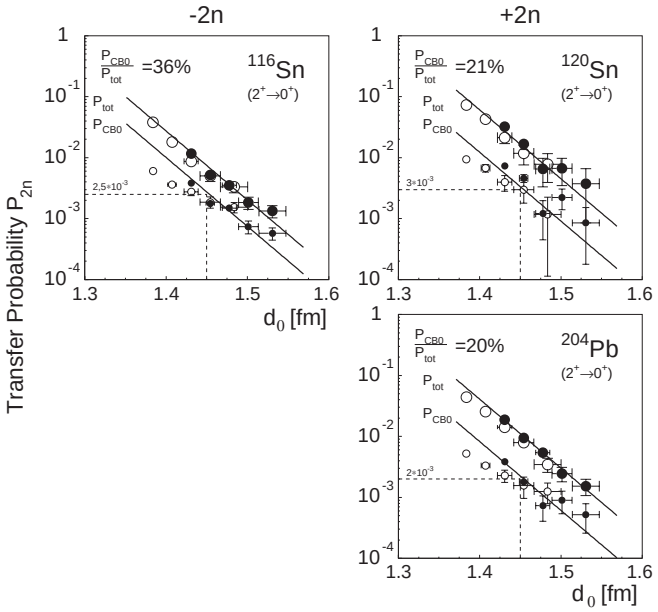

Fig. 15. Measured two-neutron transfer probabilities for the transitions selected with the $0^+ \rightarrow 2^+$ γ-decay as a function of the overlap parameter d_0 without any condition ($P_{\rm tot}$) and with the Crystal Ball in anticoincidence ($P_{\rm CB0}$). The percentage of the supra-cold component is indicated.

Here we present in table 3 only two rows for the cross-sections: namely of all states in fragment 1 (^{117}Sn) with the ground state of fragment 2 (^{207}Pb), and the second with the role of fragment 2 and fragment 1 exchanged. The calculations have been done in both directions for stripping and pick-up, seen from the ^{118}Sn as ($-$1n) and ($-$2n), or (+1n) and (+2n) transfers. These calculated cross-sections will serve to obtain transfer probabilities for the comparison with the experimental transfer probabilities obtained with the condition CB0 (CB in anticoincidence), where one of the fragments is not excited (ground state), and the feeding to the excited state is removed by demanding that no other γ-transition has occurred.

For the case of 2n transfer, as in a stripping reaction, written as a + A $\rightarrow$ b(= a $-$ 2) + B(= A + 2), we have to consider the initial channel α, the final channel β, and all intermediate channels γ corresponding to the one-particle transfer channels, c(= a $-$ 1) + C(= A + 1). This is illustrated in figs. 16 and 17. We will have, in addition to the one-step 2n transfer, a second-order sequential transfer amplitude $T^{(\rm seq)}_{\beta\alpha}$, and the non-orthogonality of the channel wave functions in the different partitions gives rise to another second-order contribution. Finally, there are the higher-order processes, which proceed via the first-excited vibrational 2^+ states in the even-mass nuclei (indirect route); these routes are also drawn in figs. 16 and 17. Explicit calculations for the 2n transfer with these indirect routes are cited in table 5. Their contribution to the absolute values turns out to be smaller mainly because they are of higher order. It is known that the coherent sum of direct and indirect routes interfere coherently, and the interference can be constructive or destructive, giving

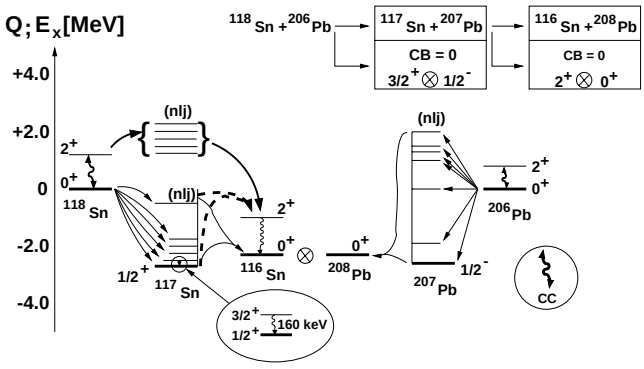

Fig. 16. Coupling scheme for 1n/2n-stripping ($-x$n) with the indication of the γ-transition used to select the fragment, and the feeding removed by the Crystal Ball (CB) in anticoincidence ($P_{\rm CB0}$). The indirect transfer routes (via the 2^+ state), as well as the sequential transfers for 2n transfer to the 0^+ and 2^+ states (the full and the dashed lines, respectively) are indicated, with and without the coupling to the vibrational states (2^+). The latter are indicated as CC for full coupling, see also fig. 17.

rise to structures in the angular distributions, see ref. [5]. In tables 4 and 5 in sect. 4.3, the cited cross-section values refer to a fixed angle. The interference is more important for the case of rotational excitations [5].

The total amplitude for the direct transfer up to second-order assumes the form [5]

$$T^{(2)}_{\beta\alpha} = T^{(1)}_{\beta\alpha} + T^{(\rm seq)}_{\beta\alpha} + T^{(\rm orth)}_{\beta\alpha}\,. \qquad (8)$$

Thus the 2n transfer will mainly proceed by two processes: i) The one-step transfer of a neutron pair, where

Table 3. Spectroscopic amplitudes (S_i) and calculated cross-sections for 1n transfer transitions between individual states in the transfer reactions ^{118}Sn + ^{206}Pb $\rightarrow$ ^{117}Sn + ^{207}Pb, and $\rightarrow$ ^{119}Sn + ^{205}Pb; $E_{\rm lab} = 606$ MeV, at $\theta_{\rm CM} = 140°$. The *spectroscopic amplitudes*, S_1 and S_2, are given by the definition $CFP = (S_i)^2$. The table shows the DWBA cross-section in [mb/sr] for the ground-state configurations (indicated in the second column) for one fragment, combined in pairs where the other partner is in typically six different states. The cross-sections include the multiplication with the appropriate factors ($S_1 \times S_2$). The numbers below the configurations are the excitation energies in MeV.

$\theta_{\rm CM} = 140°$		^{118}Sn + ^{206}Pb $\rightarrow$ ^{117}Sn + ^{207}Pb							
^{117}Sn	J^π	$s_{1/2^+}$	$d_{3/2^+}$	$h_{11/2^-}$	$g_{7/2^+}$	$d_{5/2^+}$	$f_{7/2^-}$		$\sum\sigma$
	E^x	0.0	0.160	0.310	0.710	1.180	2.050		
^{117}Sn/ ^{118}Sn	S_1	1.15	1.30	1.80	2.70	3.10	1.25		
dσ/dΩ	^{207}Pb($s_{1/2^-}$)	1.87	0.435	0.190	0.076	4.14	0.005		6.7
^{207}Pb	J^π	$p_{1/2^-}$	$f_{5/2^-}$	$g_{9/2^+}$	$i_{13/2^+}$	$j_{15/2^-}$	$d_{5/2^+}$	$s_{1/2^+}$	
	E^x	0.00	0.571	2.73	3.51	4.11	4.39	4.63	
^{207}Pb/^{206}Pb	S_2	0.8	0.35	0.98	0.70	1.20	1.10	1.10	
dσ/dΩ	^{117}Sn($s_{1/2^+}$)	1.87	0.27	0.66	0.04	0.034	0.15	0.02	3.05

$\theta_{\rm CM} = 140°$		$\rightarrow$ ^{119}Sn + ^{205}Pb								
^{119}Sn	J^π	$s_{1/2^+}$	$d_{3/2^+}$	$h_{11/2^-}$	$d_{5/2^+}$	$s_{1/2^+}$	$f_{5/2^-}$			$\sum\sigma$
	E^x	0.00	0.024	0.089	1.088	1.249	2.636			
^{119}Sn/^{118}Sn	S_1	0.53	0.72	0.85	0.38	0.33	0.33			
dσ/dΩ	^{205}Pb($f_{5/2^-}$)	1.17	0.575	4.70	1.30	0.22	0.005			7.75
^{205}Pb	J^π	$f_{5/2^-}$	$p_{1/2^-}$	$p_{3/2^-}$	$i_{13/2^+}$	$f_{7/2^-}$	$g_{9/2^+}$	$h_{9/2^-}$	$p_{1/2^-}$	
	E^x	0.00	0.002	0.262	1.011	1.726	2.69	2.73	4.63	
^{205}Pb/^{206}Pb	S_2	2.3	1.2	1.8	3.6	2.6	2.7	1.47	1.2	
dσ/dΩ	^{119}Sn($s_{1/2^+}$)	1.17	1.22	2.49	0.104	0.53	0.02	0.044	0.0044	5.5

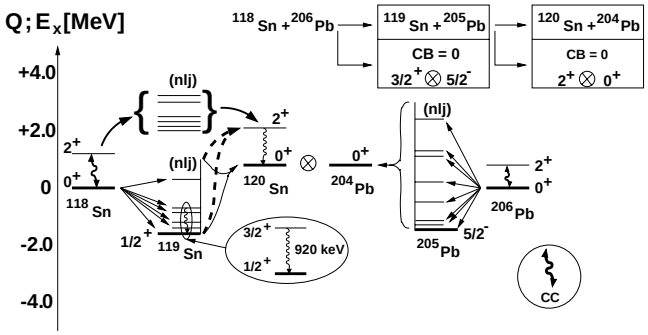

Fig. 17. Coupling scheme, as fig. 16, for 1n/2n pick-up (+xn) with the indication of the γ-transition used to select the fragment, and the direct and indirect transfer routes discussed with the CRC calculations. The solid dashed lines and the thin lines indicate the sequential transfer route to the 2^+ state and to the 0^+ state in ^{120}Sn, respectively, as in fig. 16.

the two-neutron form factor in the initial and final configurations in the two nuclei consists of sums of products of 1n wave functions (as listed in table 4); ii) The sequential transfer, which starts with an 1n transfer amplitude, with the cross-sections for the intermediate channel cited in table 3, followed by a second 1n transfer step with spectroscopic amplitudes to be taken from the second overlap. These factors can also be taken from the literature as they represent the pick-up process on the final nucleus. The sum over the individual amplitudes in the intermediate step, labelled γ, which occur in the first (1n) and the second (1n) transfer steps, creates the configuration mixing, which is finally responsible for the enhancement.

The list of single-particle configurations in tables 3 and 4 illustrates the amount of configuration mixing, which has been included in the present calculation of the 2n transfer. The same configuration mixing enters into the two-neutron form factors. It is easy to see that in cases of states with spin 0^+ and 2^+ a large number of configurations contributes.

The 2n wave function is schematically written as a superposition of products of many configurations characterised by the shell model quantum numbers (n, l, j) here with the index i, which runs over the various two-particle shell model configurations, $\phi_{i,(nlj)}(r_1)\phi_{i,(nlj)}(r_2)$, with amplitudes A_i:

$$\Phi_{\rm 2n}(0^+) \sim \sum_i A_i \left[\phi_{i,(nlj)}(r_1)\phi_{i,(nlj)}(r_2)\right]_{J=0}. \quad (9)$$

We have limited the number of configurations to typically six or seven values of (n, l, j), in both nuclei (Sn and Pb). For the configurations from two major shells with opposite parity, the 2n amplitudes are chosen with opposite sign. The final values for the amplitudes A_i chosen for

the 2n form factors are obtained from products of single-neutron wave functions (using information from ref. [31]) and are cited in table 4. We note that the $0^+ \rightarrow 0^+$ are indeed stronger than the $0^+ \rightarrow 2^+$ transitions as expected from considerations given in the introduction.

In order to calculate transfer probabilities, the elastic scattering cross-section is needed. For the calculation we have to choose an optical potential, which will describe the deviation from the Coulomb scattering. The parameters have been taken from [9], their values have little influence on the transfer probabilities calculated in first or second order (the absorption cancels out when the probabilities are calculated). However, the imaginary part strongly influences the result if a fully coupled calculation is done, as there the imaginary part enters in a non-linear way.

4.3 CRC calculations and the indirect route for 2n transfer

As already stated before, in addition to the (direct) population of the Sn(2^+) states in 2n transfer with angular momentum transfer $l = 2$ (see fig. 1), the route via the inelastic vibrational excitation in the incident channel and a subsequent $l = 0$ transfer, also called the *indirect route*, can be of importance. The relevant coupling schemes are shown in more detail in figs. 16 and 17. These figures also show the routes for the sequential 2n transfer process, where the intermediate states of the odd-mass fragments are first populated. These indirect routes are strong and conspicuous for the case of deformed states, where pronounced interference structures are observed in the angular distributions (see ref. [5] for examples). The values of these cross-sections for different coupling routes are given in table 5.

The results of the calculations can be summarised as follows. It turns out in our case that the *sequential transfer process* of two neutrons is suppressed relative to the one-step process for the 0^+ states, whereas for the 2^+ states the relative values of their contributions vary between pick-up and stripping cases. In some cases almost equal contributions are obtained, but usually they are smaller (*e.g.*, by 70%). The sum cross-sections (seq + 1step) shows the interference feature, it is always constructive for the 0^+ states, it appears sometimes smaller or larger for the 2^+ states.

The *indirect route* for the 2n transfer is calculated in the CCBA mode, which contains the vibrational coupling with the subsequent $l = 0$ transfer; it is a second- (or third-) order process and is found to be usually considerably smaller than the direct route, although the interference between the direct route and the indirect route can lead to peculiar interference patterns in the angular distributions. The interference of the direct and indirect routes turns out to be different for stripping and pick-up processes as already noted before [5], the result for the sum is often smaller than the direct route alone.

The indirect route and the related interference are, however, more pronounced in the case of rotational coupling, and at higher energies, where the excitation probabilities are much larger. A case for very heavy nuclei like ours, but with rotational coupling, is discussed in refs. [5,16].

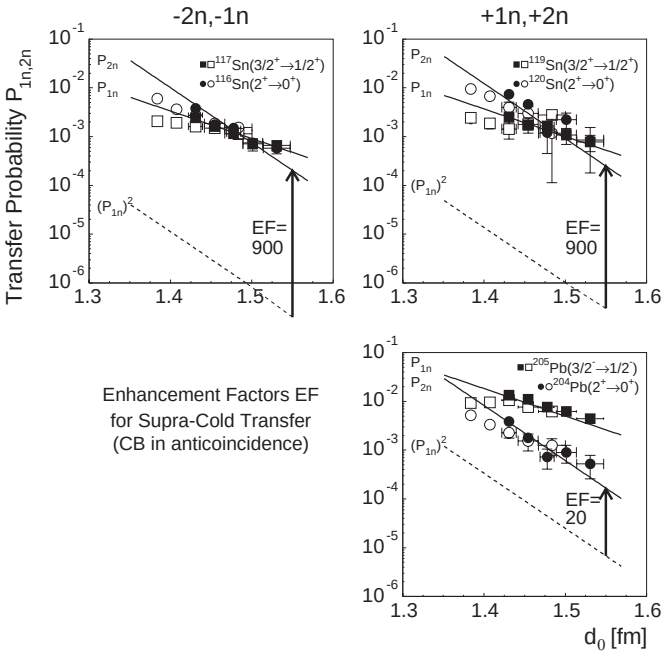

Fig. 18. One-neutron (P_{1n}) and two-neutron (P_{2n}) transfer probabilities as a function of the overlap parameter d_0 with the Crystal Ball in anticoincidence (CB0). The left column shows the neutron transfer from Sn to Pb, the right column vice versa. Filled symbols refer to a bombarding energy of 5.14 MeV/u, open symbols to 5.32 MeV/u. The nuclei are identified by the characteristic γ-transitions indicated in figs. 5 and 6. The continuous lines show the theoretically predicted slopes, the dashed lines represent the calculated square of the 1n transfer probabilities. The shift observed between the square of the 1n transfer probability and the corresponding 2n transfer probability defines the enhancement factor EF.

4.4 Results on enhancement

From the calculations of the 1n and 2n cross-sections we obtain the theoretical transfer probabilities, and these can be compared with the measured values. The absolute values for the single-neutron transfer may vary by a larger factor for different configurations, thus the calculated enhancement will depend on the choice of the 1n transition. However, for the relatively strong transitions, we find that they represent well average values, although they are often larger then average. Thus for the single-particle configurations we find for ^{117}Sn($d_{3/2}$) a differential cross-section of 0.435 mb/sr at the angle of $\theta_{\rm cm} = 140°$, for the the single-particle state in ^{207}Pb($f_{5/2}$) the differential cross-section is 0.27 mb/sr, and for the state in ^{119}Sn($d_{5/2}$) a value of 1.30 mb/sr is found, which is somewhat higher than the average. The square of the single-neutron transfer probability enters into the determination of enhancement, as can be seen in table 6 the EF factor can thus easily be

Table 4. Spectroscopic amplitudes and calculated cross-sections for two-neutron transfers to 0^+ and 2^+ states in the transfer reactions ^{118}Sn + ^{206}Pb $\rightarrow^{116}$Sn + ^{208}Pb and $\rightarrow^{120}$Sn + ^{204}Pb at $E_{\rm lab} = 606$ MeV at $\theta_{\rm CM} = 140^\circ$. The products of *spectroscopic amplitudes* at the two-neutron overlaps (Sn/Sn) and (Pb/Pb) denoted as A_1 and A_2 (A_1^* and A_2^* for the excited 2^+ states, respectively), are given. The table shows for each coupling route the DWBA cross-section in [mb/sr]. The cross-sections for the direct (d) and indirect (ind) route are given, as well as the (coherent) sum. The differential cross-section in the incident channel, the elastic scattering, is 183 mb/sr.

$\theta_{\rm CM} = 140^\circ$		$(-2n)$ ^{118}Sn$_{0^+}$+^{206}Pb$_{0^+}$ $\rightarrow$ ^{116}Sn$^\pi_J$ + ^{208}Pb$_{0^+}$						
^{116}Sn/ ^{118}Sn	$(n,l,j)^2$	$s_{1/2^+}$	$d_{3/2^+}$	$h_{11/2^-}$	$g_{7/2^+}$	$d_{5/2^+}$	$g_{7/2^+}$	
A_1	0^+	-1.1	-1.70	$+3.30$	-7.3	-5.1	-1.5	
^{116}Sn$^*(2^+)$/ ^{118}Sn	(n,l,j)	$s_{1/2^+}/d_{3/2^+}$	$d_{3/2^+}$	$h_{11/2^-}$	$g_{7/2^+}$	$d_{5/2^+}$	$g_{7/2^+}$	
A_1^*	2^+	-1.5	-1.70	$+3.30$	-7.3	-5.1	-1.5	
^{208}Pb/ ^{206}Pb	$(n,l,j)^2$	$p_{1/2^-}$	$f_{5/2^-}$	$g_{9/2^-}$	$i_{13/2^+}$	$j_{15/2^-}$	$d_{5/2^+}$	$s_{1/2^+}$
A_2	0^+	$+0.64$	$+0.12$	-0.97	-0.48	$+1.45$	-0.77	-1.1
dσ/dΩ ^{208}Pb(0^+)	^{116}Sn$_{0^+}$	^{116}Sn$_{2^+}$		^{116}Sn$_{2^+}$, ind		^{116}Sn$_{2^+}$, d + ind		
[mb/sr]	8.75	0.73		1.1		2.34		

$\theta_{\rm CM} = 140^\circ$		$(+2n) \rightarrow$ ^{120}Sn$^\pi_J$ + ^{204}Pb$_{0^+}$					
^{120}Sn/ ^{118}Sn	$(n,l,j)^2$	$s_{1/2^+}$	$d_{3/2^+}$	$h_{11/2^-}$	$g_{7/2^+}$	$d_{5/2^+}$	$s_{1/2^+}$
A_1	0^+	$+0.38$	$+0.91$	-1.6	$+0.6$	$+1.44$	$+0.15$
^{120}Sn$^*(2^+)$/ ^{118}Sn	(n,l,j)	$s_{1/2^+}/d_{3/2^+}$	$d_{3/2^+}$	$h_{11/2^-}$	$g_{7/2^+}$	$d_{5/2^+}$	s_{12^+}
A_1^*	2^+	$+0.90$	0.91	-1.7	$+0.6$	$+1.44$	$+0.15$
^{206}Pb/^{204}Pb(0^+)	$f_{5/2^-}$	$p_{1/2^-}$	$p_{3/2^-}$	$i_{13/2^+}$	$f_{7/2^-}$	$h_{9/2^-}$	$g_{9/2^+}$	$s_{1/2^+}$
$(n,l,j)^2$, A_2	-1.15	-1.11	-0.68	$+1.1$	-0.49	-1.6	$+2.16$	$+0.11$
dσ/dΩ ^{204}Pb(0^+)	^{120}Sn$_{0^+}$	^{120}Sn$_{2^+}$		^{120}Sn$_{2^+}$, ind		^{120}Sn$_{2^+}$, d + ind	
[mb/sr]	0.876	0.289		0.016		0.28	

Table 5. Cross-section from CRC calculations with the sequential and one-step coupling routes for the population of states in Sn isotopes, (with the intermediate states of the odd-mass isotopes as illustrated in figs. 16 and 17), and for the indirect routes via the inelastic couplings via the 2^+ states. Two directions (pick-up and stripping) for the 1n and 2n transfer reactions $(-2n)$, ^{118}Sn + ^{206}Pb $\rightarrow^{117}$Sn + ^{207}Pb ($\rightarrow^{116}$Sn + ^{208}Pb), and $(+2n)$, $\rightarrow^{119}$Sn + ^{205}Pb ($\rightarrow^{120}$Sn + ^{204}Pb) are considered at an energy of $E_{\rm lab} = 606$ MeV and $\theta_{\rm CM} = 140^\circ$. These values are to be compared with those cited in tables 4 and 6. The sum of the one-step plus the sequential process is also given.

$\theta_{\rm CM} = 140^\circ$	Cross-sections for different coupling routes			
dσ/d$\Omega(+2n)$	^{120}Sn(0^+)	^{120}Sn(2^+)	^{120}Sn(0^+)	^{120}Sn(2^+)
sequ/[mb/sr]	0.414	0.078	0.519(seq + 1step)	0.134(seq + 1step)
dir/indir	0.876(d)	0.289(d)	0.0(ind)	0.01(ind)
dσ/d$\Omega(-2n)$	^{116}Sn(0^+)	^{116}Sn(2^+)	^{116}Sn(0^+)	^{116}Sn(2^+)
sequ/[mb/sr]	0.38	0.70	8.8(seq + 1step)	0.81(seq + 1step)
dir/indir	8.75(d)	0.78(d)	0.038(ind)	0.002(ind)

different by a factor 10. For the values, which are representative for the average 1n transfer process, the determination of the enhancement from the calculations agrees satisfactorily with the experimental result. The calculated transfer probabilities are derived using the elastic cross-sections obtained simultaneously, which is also given the compilation in table 6.

The calculated values of the probabilities for 1n and 2n transfers agree quite well with the experimental result. We cite some values of the transfer probabilities (including the ground states, for which no data have been obtained) at a distance parameter $d_0 = 1.45$ fm, and compare to the data given in the figures and in the tables:

^{117}Sn: exp $2.0 \cdot 10^{-3}$; calc $2.3 \cdot 10^{-3}$,
^{116}Sn(0^+): exp – ; calc $4.7 \cdot 10^{-2}$,
^{116}Sn(2^+): exp $2.3 \cdot 10^{-3}$; calc $4.0 \cdot 10^{-3}$,
^{119}Sn: exp $3.0 \cdot 10^{-3}$; calc $7.0 \cdot 10^{-3}$,
^{120}Sn(0^+): exp – ; calc $6.5 \cdot 10^{-3}$,
^{120}Sn(2^+): exp $6.0 \cdot 10^{-3}$; calc $4.0 \cdot 10^{-3}$.

Table 6. Calculated enhancements EF and transfer probabilities for transitions chosen as individual states for the determination of EF. Two directions (pick-up and stripping) for the 1n and 2n transfer reactions ($-$2n), ^{118}Sn + ^{206}Pb $\rightarrow$^{117}Sn + ^{207}Pb ($\rightarrow$^{116}Sn + ^{208}Pb), and (+2n) $\rightarrow$^{119}Sn + ^{205}Pb ($\rightarrow$^{120}Sn + ^{204}Pb) are considered at an energy of $E_{\rm lab}$ = 606 MeV, and $\theta_{\rm CM} = 140^\circ$. These values must be compared with the experimental values given in figs. 18 The enhancement factor EF is given with the definition $EF = (P_{2n})/(P_{1n})^2$. The values for 2n transfer are also given for the non-observed for 0^+ to 0^+ transitions, the values for to 2^+ states in Sn_{2^+} or Pb_{2^+} are with the other fragment in the ground state.

$\theta_{\rm CM} = 140^\circ$	Calc. cross-sections, Transfer Probabilities and Enhancements (EF),^{118}Sn + ^{206}Pb					
$d\sigma/d\Omega$(1n)	^{118}Sn(0^+)	^{117}Sn($3/2^+$)	^{119}Sn($5/2^+$)	^{207}Pb($5/2^-$)	^{205}Pb($3/2^-$)	^{205}Pb($7/2^-$)
[mb/sr]	183.3	0.435	1.30	0.27	2.5	0.53
$P_{\rm tr}$	–	0.0023	0.007	0.0014	0.013	0.0029
$d\sigma/d\Omega$(2n)	^{116}Sn(0^+)	^{116}Sn(2^+)	^{120}Sn(2^+)	^{120}Sn(0^+)	^{204}Pb(2^+)	^{204}Pb(0^+)
[mb/sr]	8.75	0.73	0.29	0.289	1.2	0.876
$P_{\rm tr}$	0.047	0.004	0.00163	0.0048	0.0065	0.0048
EF,calc	1000	1000	33	10	38	28
EF,exp	–	900	900	–	20	–

The comparison gives a very satisfactory result considering the uncertainties, which enter through the choice of the bound-state parameters for the 1n and 2n wave functions and the spectroscopic amplitudes. Similarly, the uncertainties in the data related to the efficiency of the anticoincidence selection (CB0), will give experimental cross-sections which in some cases may be too large by a factor 2.

For the discussion of the enhancement EF, we can neglect the effects of the indirect routes, as shown by the results of the calculations. For the determination of EF our result with the chosen states can be considered as typical for 1n and 2n transfer probabilities. We find from the present analysis that we can directly use the experimentally selected 1n and 2n transfers, and the enhancement factors are given in table 6. The agreement is very satisfactory for two cases, and the deviations can easily be understood in terms of particular values of the single-neutron transfer probabilities. Thus, for example, for the ^{205}Pb nucleus the cross-section for two different 1n transfers are cited, the EF being determined only with one, the larger cross-section, which evidently results in a smaller value of EF.

5 Conclusions

In this work we were able to measure for the first time with a unique set-up consisting of the Euroball Clusters and the Heidelberg-GSI-Crystal Ball for γ-ray detection and position-sensitive charged-particle detectors, neutron transfer transitions between well-defined states for a very heavy system consisting of super-fluid spherical nuclei. The system ^{206}Pb + ^{118}Sn has been chosen in order to search for a large enhancement in 2n transfer between the ground and low-lying states of even-even nuclei, which is expected for neutron transfer between two nuclei with super-fluid properties [7]. With this experimental technique it was possible to obtain the microscopic enhancement related to the comparison of the square of the single-neutron transfer strength for a typical single-particle state, with the 2n transfer strength for a separated super-fluid state. The selection of the well-defined single- and 2n neutron transfer transitions was possible with the particle-γ coincidence technique and the Crystal Ball in anticoincidence, removing the feeding from higher-lying states. Thus transitions to levels in the odd isotopes were observed, which represent typical values for the single-particle strength. The observed transfers imply the ground-state to ground-state transition in one vertex, and the ground-state to the excited-state one (with the characteristic γ-decay) for the second vertex. For the 2n transfer the transitions to the lowest 2^+ states in ^{120}Sn, ^{116}Sn and ^{204}Pb were measured. For these states also an enhancement similar to the ground-state $\rightarrow$ ground-state transitions in the partner ("recoil") nuclei is expected. The data imply the observation of the product of two enhanced transitions in two vertices, in the ground-state to ground-state transition (fragment 1) in one vertex, and the ground-state to 2^+-state transition in the partner (fragment 2) vertex. The values of the *microscopic enhancement* observed are EF = 1000 for two cases as predicted in ref. [7] for a combination of two pure ground-state to ground-state transitions.

It turns out that the cases described here, with the observation of 2^+ states in one vertex, give a similar enhancement as for the 0^+ to 0^+ transitions. This observation is quantitatively reproduced in CRC calculations for the 2n transfer. The configuration mixing in the 2^+ states is very similar to that found in the 0^+ states. The calculations suggest that the transfer in the vertex with the 2^+ states proceeds in a mixture of one-step and sequential processes. The calculations also show that the indirect route proceeding via a vibrational excitation is small.

As discussed in the introduction, the *macroscopic enhancement* is often studied without separation of individual states. From our result, we can conclude that the values in these cases contain a big contribution from populations of both the 0^+ and the 2^+ transitions. The related 1n transfer strength for these macroscopic enhancements is

the sum over the single-particle strength. We can partially deduce the global 1n transfer probability from our "raw" data and from the summed cross-sections, $\sum\sigma$, in table 3. With these definitions the macroscopic enhancement reaches only values of 2 to 10 (see also refs. [5,32]). At higher energies and in some other cases of normal nuclei discussed also in ref. [5], the experimentally defined macroscopic enhancement turns out to be exactly equal to 1, because at higher energies the full space of single- and two-particle configurations is populated. In multi-neutron transfer then a continuous exponential slope for the subsequent single and two-neutron transfers is observed [32].

We conclude that the experimental method with the highly effective multiplicity filter used here is a powerful approach to study reaction mechanisms in reactions with very heavy ions, where charged-particle spectroscopy is far away from the possibility to determine the quantum states of reaction fragments. The future use of such setups with larger segmented gamma-detector arrays thus appears rather promising for nuclear-reaction studies.

This work has been supported by the GSI under contract No. OBOEK, and partially by the German Ministry of Research (BMFT, Verbundforschung, under contract 06OB472D/4). We are indebted to the German EUROBALL Collaboration for providing the Euroball Cluster detectors. Particular thanks are due to the Crystal Ball groups of GSI-Darmstadt and MPI-Heidelberg, which made these experiments possible. Support in the UK is acknowledged from EPSRC grants GR/R/59670 and GR/M/82141. One of the authors (W.vOe) takes the opportunity to thank the Department of Physics at University of Surrey in Guildford for the hospitality extended to him in the winter term 2001/2002.

References

1. R.A. Broglia, O. Hansen, C. Riedel, in *Advances in Nuclear Physics*, edited by M. Baranger, E. Vogt, Vol. **6** (Plenum Press, New York, 1973) p. 287.
2. R.A. Broglia, Ann. Phys. (N.Y.) **80**, 60 (1973).
3. R.A. Broglia, C. Riedel, B. Sorensen, Nucl. Phys. A **115**, 273 (1968).
4. W. von Oertzen, in *Nuclear Collisions from the Mean Field into the Fragmentation Regime*, in *Proceedings of the International School of Physics Enrico Fermi, Course CXII*, edited by C. Détraz, P. Kienle (North Holland, Amsterdam, 1991), p. 459; W. von Oertzen, in *Probing the Nuclear Paradigm with Heavy Ion Reactions, Erice School (I), 1993*, edited by R.A. Broglia *et al.*, (World Scientific, Singapore, 1994) p. 29.
5. W. von Oertzen, A. Vitturi, Rep. Prog. Phys. **64**, 1247 (2001).
6. C.H. Dasso, A. Vitturi (Editors), SIF Conf. Proc., Vol. **18**, *Collective Aspects in Pair-Transfer Phenomena, Varenna, Italy, 1987* (Editrice Compositori, Bologna, 1989).
7. R.A. Broglia *et al.*, Phys. Lett. B **73**, 401 (1978).
8. R.A. Broglia, A. Winther, *Heavy Ion Reactions, Lecture Notes* (Addison Wesley Publ. Comp., Redwood, 1991).
9. W. von Oertzen *et al.*, Z. Phys. A **326**, 463 (1987).
10. W. von Oertzen, Phys. Rev. C **43**, R1522 (1991).
11. W. von Oertzen, *Cold multinucleon transfer and synthesis of new elements*, in *Heavy Elements and Related Phenomena*, edited by R.K. Gupta, W. Greiner, Vol. **1** (World Scientific, Singapore, 1999) p. 68.
12. C.Y. Wu, W. von Oertzen, D. Cline, M. Guidry, Ann. Rev. Nucl. Part. Sci. **40**, 285 (1990).
13. D.C. Cline, Nucl. Phys. A **520**, 493c (1990).
14. D. Schwalm, in *Probing the Nuclear Paradigm with Heavy Ion Reactions, Erice School (I), 1993*, edited by R.A. Broglia *et al.* (World Scientific, Singapore, 1994) p. 29.
15. J.O. Rasmussen *et al.*, Phys. Rep. C **264**, 325 (1996).
16. T. Härtlein *et al.*, Eur. Phys. J. A **4**, 41 (1999); H. Bauer, Thesis, University of Heidelberg, Max Planck Institut für Kernphysik, MPI H-V40, 1998.
17. S.J. Sanders *et al.*, Phys. Rev. C **55**, 2541 (1997).
18. I. Peter *et al.*, Eur. Phys. J. A **4**, 313 (1999).
19. W.J. Kernan *et al.*, Nucl. Phys. A **524**, 344 (1991).
20. V. Metag, D. Habs, D. Schwalm, Nucl. Part. Phys. **16**, 213 (1986).
21. I. Talmi, *Simple Models of Complex nuclei, Contempory Concepts in Physics*, Vol. **7** (Harwood Academic Publishers, Chur, 1993) pp. 473ff.
22. F. Iachello, Nucl. Phys. A **570**, 145c (1994).
23. M. Igarashi, K.I. Kubo, Phys. Rep. **199**, 1 (1991).
24. J. Speer *et al.*, Phys. Lett. B **259**, 422 (1991).
25. Th. Wilpert *et al.*, Z. Phys. A **358**, 395 (1997).
26. I. Peter, PhD Thesis, Freie University Berlin, 1998.
27. K. Vetter *et al.*, Nucl. Instrum. Methods A **344**, 607 (1994).
28. J. Blachot, G. Marguier, Nucl. Data Sheets **75**, 99 (1995); R.G. Helmer, M.A. Lee, Nucl. Data Sheets **61**, 93 (1990).
29. H.J. Wollersheim, Habilitationschrift (1993), GSI Scientific Report GSI-93-22.
30. I.J. Thompson, Comput. Phys. Rep. **7**, 167 (1988).
31. M.J. Martin, Nucl. Data Sheets **70**, 315 (1993); S. Rab, Nucl. Data Sheets **69**, 679 (1993).
32. L. Corradi *et al.*, Phys. Rev. C **63**, 021601 (2001) and references therein.